Effect of Rapid Infrared Annealing on the Photoelectrochemical Properties of Anodically Fabricated TiO 2 Nanotube Arrays

ARTICLE *in* THE JOURNAL OF PHYSICAL CHEMISTRY C · MAY 2009

Impact Factor: 4.77 · DOI: 10.1021/jp902140d

THE JOURNAL OF PHYSICAL CHEMISTRY LETTERS

2009, *113,* 7996–7999
Published on Web 04/22/2009

Effect of Rapid Infrared Annealing on the Photoelectrochemical Properties of Anodically Fabricated TiO_2 Nanotube Arrays

Nageh K. Allam*,† and Craig A. Grimes*,†,‡

The Department of Materials Science and Engineering and The Department of Electrical Engineering, The Pennsylvania State University, University Park, Pennsylvania 16802

Received: March 10, 2009; Revised Manuscript Received: April 14, 2009

A significant enhancement in the photoconversion efficiency of anodically grown titania nanotube array photoanodes is observed when crystallized using an infrared annealing process. This infrared (IR) annealing treatment is performed over relatively short periods, 5−15 min, over the temperature range 300−600 °C with the anatase crystallite size increasing with annealing temperature and duration. Used as photoanodes to photoelectrochemically split water, the 15 min, 600 °C IR crystallized nanotube arrays show a three-electrode photoconversion efficiency of 13.13% under UV illumination (100 mW/cm^2, 320−400 nm, 1 M KOH). A reduction in the carrier trap states and an increased charge carrier transport due to reduction of the barrier layer thickness are believed responsible for the significant conversion efficiency seen with the IR annealed samples.

Introduction

TiO_2 is an important semiconductor material used in various applications including gas sensing,[1] marine pollution control,[2] photocatalysis,[3] and solar energy applications.[4−8] For all of these applications, crystallinity, stability, and purity are particularly important. TiO_2 has three primary crystalline polymorphs: rutile, anatase, and brookite.[9] Recently, these nanocrystalline polymorphs of TiO_2 have been intensively studied since their physicochemical properties have been found to be superior to their bulk.[3] Thermodynamically, the rutile phase is the most stable form that has been widely investigated because of its chemical stability and high refractive index of 2.7 at 500 nm.[10] However, the anatase phase exhibits photocatalytic and solar energy properties superior to those of rutile[11] with anatase and rutile mixtures showing catalytic efficiencies depending on their relative ratio in the mixture.[12]

The one-step electrochemical anodization method recently proposed by Grimes and co-workers[13] provides a unique route for fabricating large-scale highly ordered and vertically oriented TiO_2 nanotube arrays.[14−21] These titania nanotube arrays, synthesized by anodization of a Ti thick film, are commonly amorphous with an elevated temperature heat-treatment used to induce crystallinity, typically at temperatures ≥450 °C for 3−6 h.[22] Extended, high temperature anneals lead to the formation of a thick barrier layer that separates the nanotube array film from the underlying metal substrate.[22,23] This barrier layer has been shown to be composed mainly of rutile crystallites with some nonstoichiometric oxides that can act as carrier trap states.[22,24,25] In regard to photoelectrochemical water splitting,[26−28] the barrier layer acts to hinder electron transfer to the metal electrode (cathode) where water reduction takes place, in turn reducing the overall water splitting efficiency. Moreover, the need for a high-temperature anneal of extended duration to achieve crystallization limits use of the nanotube arrays with temperature-sensitive materials.

Herein we report the use of infrared (IR) annealing, which is both a facile and novel method to fabricate crystalline TiO_2 nanotube arrays in which the nanotube arrays are exposed to temperatures up to 600 °C for 5 to 15 min. IR-annealed samples demonstrate photoelectrochemical properties comparable or superior to their thermally annealed counterparts due, we believe, to the limited formation of a barrier layer and improved nanotube crystallinity that in turn reduces recombination losses.[29,30]

Experimental Section

Pure titanium foil (0.25 mm thick) was purchased from Sigma Aldrich. Rectangular samples (1.5 × 1.5 cm) were cleaned with acetone followed by a deionized (DI) water rinse then anodized using a two-electrode cell with the titanium foil as the working electrode and platinum foil as the counter electrode under constant applied voltage at room temperature (≈22 °C) at 20 V for 20 h in a formamide-based electrolyte containing 0.2 M NH_4F, 0.1 M H_3PO_4, and 3 vol % H_2O. The as-anodized samples were rinsed with DI water and dried using a nitrogen stream. The TiO_2 nanotube arrays were crystallized by subjecting them to infrared annealing using a RTC infrared furnace (LA 306) at 300, 400, 500, and 600 °C for time intervals of 5, 7, 10, and 15 min under air ambient with a flow rate of 50 standard cubic feet per hour (SCFH). The crystalline phases were detected and identified by a glancing angle X-ray diffractometer (GAXRD) on a Philips X'pert MRD PRO X-ray diffractometer (Almelo, The Netherlands). Sample morphology was examined using a JEOL JSM-6300 field emission scanning electron microscope (FESEM).

The photoelectrochemical properties of the crystallized nanotube arrays were investigated using a three-electrode configu-

* To whom correspondence should be addressed. E-mail: (C.A.G.) cgrimes@engr.psu.edu; (N.K.A.) Nageh.Allam@gmail.com.
† The Department of Materials Science and Engineering.
‡ The Department of Electrical Engineering.

10.1021/jp902140d CCC: $40.75

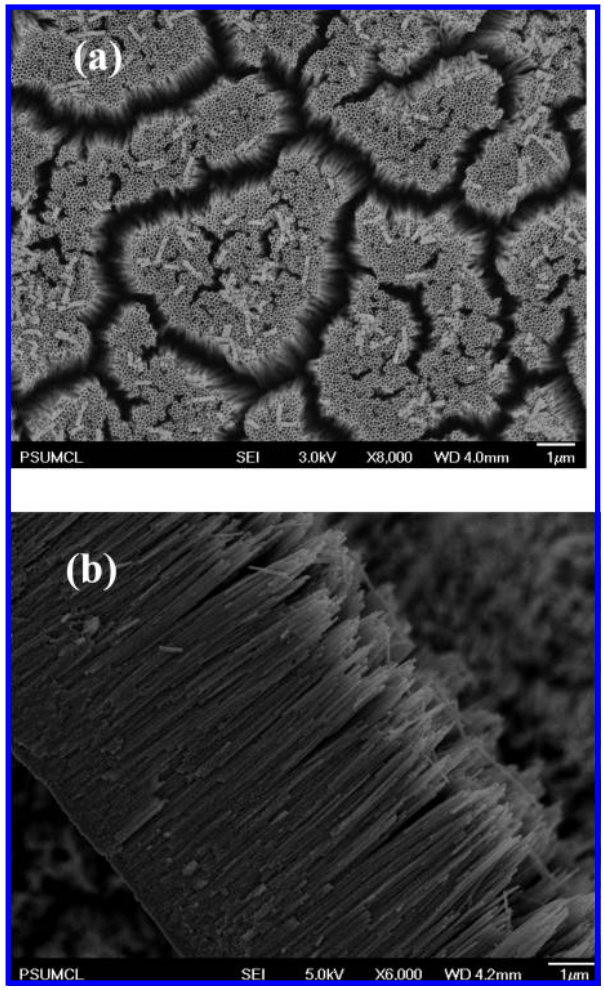

Figure 1. (a) FESEM top-view image of the fabricated TiO_2 nanotube arrays upon anodizing Ti foil, 250 μm thick, in a formamide-based electrolyte containing 0.2 M NH_4F, 0.1 M H_3PO_4, and 3 vol % H_2O at 20 V for 20 h; (b) the corresponding cross sectional view.

ration with a TiO_2 nanotube array working electrode, saturated Ag/AgCl as a reference electrode, and platinum foil as a counter electrode. A 1.0 M KOH solution was used as the electrolyte. A scanning potentiostat (CH Instruments, model CHI 600B) was used to measure dark and illuminated currents at a scan rate of 10 mV/s. A 50 W metal halide lamp (Exfo Lite) was used as the light source with optical filters used to restrict the incident light to UV wavelengths between 320 and 400 nm. The incident power was determined as 100 mW/cm^2 using a thermopile detector (Spectra Physics, CA) after eliminating the light reflection and absorption effects at the Pyrex glass window.

Results and Discussion

Figure 1a shows an FESEM top view image of nanotube arrays synthesized by anodizing Ti foil at 20 V for 20 h in a formamide-based electrolyte containing 0.2 M NH_4F, 0.1 M H_3PO_4, and 3% H_2O. The fabricated nanotubes were found to be 7 $\pm$ 0.2 μm in length (see Figure 1b). Details on the TiO_2 nanotube array formation have been previously reported.[15,31] GAXRD patterns of the IR annealed TiO_2 nanotube array films at different temperatures (300 to 600 °C) for different time intervals (5 to 15 min) indicate a crystalline nature for all samples annealed at temperatures $\geq$400 °C for 5 min or more. We limited the IR annealing time to a maximum of 15 min since annealing at 600 °C for 30 min leads to collapse of the tubular structure.

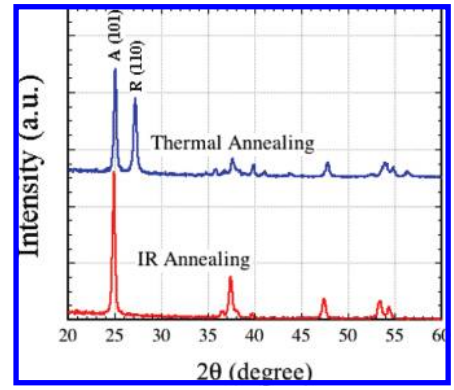

Figure 2. 2° GAXRD patterns of 7 μm long TiO_2 nanotube arrays thermally (600 °C, 4 h) and IR (600 °C, 15 min) annealed.

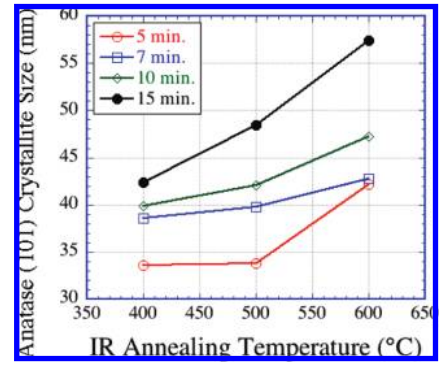

Figure 3. Variation of anatase crystallite size as a function of IR annealing temperature and time.

Figure 2 compares the GAXRD diffraction pattern obtained from two typical IR and thermally annealed samples. The rutile signature for the thermally annealed sample is due, we believe, to the relatively thicker barrier layer. IR annealing appears efficient in terms of ease, time, and performance through formation of a minimal barrier layer that in turn facilitates electron transfer to the metal electrode (cathode). Note that rapid thermal anneals of similar samples at 600 °C for 15 min generally resulted in detachment of the nanotube array film from the underlying Ti foils substrate.

To investigate the influence of the anatase crystallite size (D) on the behavior of the IR-crystallized nanotube arrays, the variation of the size of the anatase crystallites with temperature, Figure 3, was estimated using the following Scherrer formula[32]

$$D = \frac{0.9\lambda}{\mathrm{FWHM}\cos(\theta)} \quad (1)$$

where λ is the wavelength of Cu Kα radiation (1.5418 Å), 0.9 is the Scherrer constant, θ is the Bragg reflection angle, and FWHM is the full-width at half-maximum intensity of the anatase (101) peak. The relative standard deviation of the determined average particle size is ~7%. The instrument broadening was corrected for using NIST 640c silicon. It can be seen that the anatase crystallite size progressively increased with temperature after its nucleation.

Anatase has two low energy surfaces, (101) and (001); however, the (101) surface is the most prevalent face for anatase nanocrystals.[33] Figure 4 shows the variation in the anatase (101) peak intensity with IR annealing duration and temperature. The intensity of the (101) peak increases with both anneal duration and temperature. No rutile is apparent in the GAXRD patterns of the IR annealed samples for 5−15 min. After a 4 h IR anneal, we have detected rutile reflections; however, we do not have

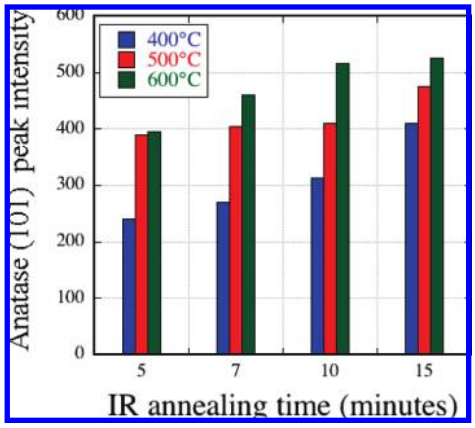

Figure 4. Change of anatase (101) peak intensity measured via 2° glancing angle X-ray diffraction (GAXRD) for the IR-annealed samples as a function of annealing time and temperature.

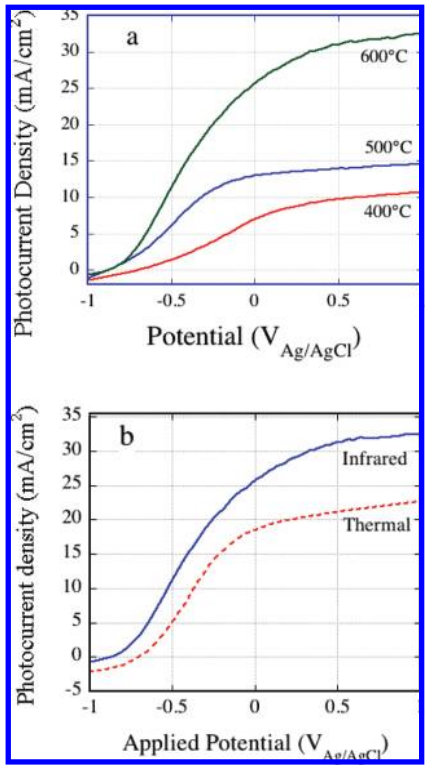

Figure 5. Photocurrent density vs potential in 1 M KOH solution under UV (320−400 nm, 100 mW/cm^2) illumination for (a) IR-annealed thermally 7 μm long TiO_2 nanotube array samples for 15 min at different annealing temperature, and (b) thermally (600 °C, 4 h), and IR (600 °C, 15 min) annealed 7 μm long TiO_2 nanotube array samples.

tubes anymore due to structural collapse. With the short IR anneals, the rutile layer, we believe, simply does not have time to grow to a thickness great enough to give a significant XRD signal. It is known from previous studies that the nanotube walls are anatase, and the thermally oxidized metal layer underneath the nanotubes is mainly rutile.[22] The thickness of the barrier layer formed with a 600 °C 15 min IR anneal is approximately 200 nm. In contrast, a 600 °C 4 h thermal anneal results in a barrier layer approximately 1.4 μm thick. That is to say, we can only do this for short durations, and the rutile layer does not have time to form.

Figure 5a shows the measured photocurrent density versus potential in 1 M KOH under 320−400 nm, 100 mW/cm^2 illumination of IR annealed 7 μm long nanotube arrays for 15 min duration as a function of temperature. Figure 5b shows the photocurrent density versus potential in 1 M KOH solution under UV (320−400 nm, 100 mW/cm^2) illumination for thermally (600 °C, 4 h), and IR (600 °C, 15 min) annealed 7 μm long TiO_2 nanotube array samples. As seen in Figure 5b, the photocurrent in the IR-annealed sample is significantly greater than that of the thermally annealed sample due, we believe, to the thinner barrier layer and improved crystallinity.

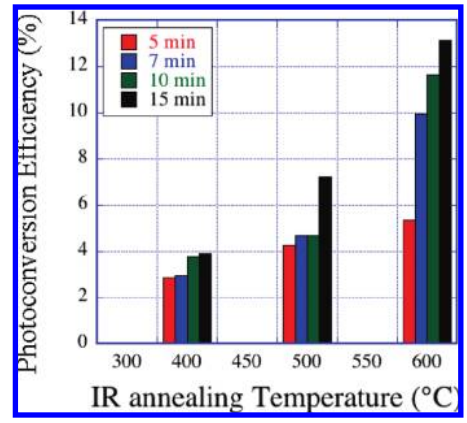

Figure 6. Change in photoconversion efficiency of the IR-annealed 7 μm long TiO_2 nanotube array photoanodes, measured in 1 M KOH under 100 mW/cm^2 320−400 nm illumination, as a function of annealing time and temperature.

The light energy to chemical energy conversion (photoconversion) efficiency η was calculated as follows[28,34]

$$\eta\,\% = [(\text{total power output} - \text{electrical power output})/\text{light power input}] \times 100$$
$$= j_p[(E^0_{rev} - |E_{appl}|)/I_0] \times 100 \quad (2)$$

where j_p is the photocurrent density (mA/cm^2), $j_pE^0_{rev}$ is the total power output, $j_p|E_{appl}|$ is the electrical power input and I_0 is the power density of incident light (mW/cm^2). E^0_{rev} is the standard reversible potential which is 1.23 V_{NHE} and the applied potential $E_{appl} = E_{meas} - E_{aoc}$, where E_{meas} is electrode potential (versus Ag/AgCl) of the working electrode at which photocurrent was measured under illumination and E_{aoc} is the electrode potential (versus Ag/AgCl) of the same working electrode at open circuit conditions under same illumination and in the same electrolyte.

As indicated in Figure 6, the photoconversion efficiencies for the IR-crystallized nanotube arrays increase with both annealing temperature and time, generally tracking the variation in anatase (101) intensity as seen in Figure 4. The highest photoconversion efficiency of ≈13.13%, see Figure 5b, was obtained for the 7 μm long TiO_2 nanotube arrays annealed at 600 °C for 15 min, a value significantly greater than that obtained for the 7 μm thermally annealed nanotube array sample, 600 °C for 4 h with 1 °C/min rate of change, which showed a photoconversion efficiency of η = 10%.

Conclusions

In conclusion, a novel method is reported for fabrication of crystalline TiO_2 nanotube arrays synthesized by Ti anodization. Infrared annealing is found to be an efficient technique for crystallizing the nanotube array films within a few minutes. The IR-annealed nanotube array films, used as photoanodes to photoelectrochemically split water under UV illumination (320−400 nm), showed significant photoconversion efficiencies (η = 13.13% for 7 μm long nanotubes). It is noteworthy mentioning that we are now in the process of adapting the

infrared annealing technique for other systems such as our recently fabricated Ta_2O_5 nanotubes[35] as well as other nanotube array systems.[2]

Acknowledgment. Support of this work by the Department of Energy under Grant DE-FG02-06ER15772 is gratefully acknowledged.

References and Notes

(1) Paulose, M.; Varghese, O. K.; Mor, G. K.; Grimes, C. A.; Ong, K. G. *Nanotechnology* **2006**, *17*, 398.
(2) Grimes, C. A.; Mor, G. K. *Ti_2O Nanotube Arrays: Synthesis, Properties, and Applications*; Springer: Norwell, MA, 2009.
(3) Linsebigler, A. L.; Lu, G.; Yates, J. T. *Chem. Rev.* **1995**, *95*, 735.
(4) Mor, G. K.; Shankar, K.; Paulose, M.; Varghese, O. K.; Grimes, C. A. *Nano Lett.* **2006**, *6*, 215.
(5) Thompson, T. L.; Yates, J. T. *Chem. Rev.* **2006**, *106*, 4428.
(6) Zhu, K.; Neale, N. R.; Miedaner, A.; Frank, A. J. *Nano Lett.* **2007**, *7*, 69.
(7) Mor, G. K.; Shankar, K.; Paulose, M.; Varghese, O. K.; Grimes, C. A. *Appl. Phys. Lett.* **2007**, *91*.
(8) Allam, N. K.; Shankar, K.; Grimes, C. A. *J. Mater. Chem.* **2008**, *18*, 2341.
(9) Gribb, A. A.; Banfield, J. F. *Am. Mineral.* **1997**, *82*, 717.
(10) Yoo, D.; Kim, I.; Kim, S.; Hahn, C. H.; Lee, C.; Cho, S. *Appl. Surf. Sci.* **2007**, *253*, 3888.
(11) Fujishima, A.; Rao, T. N.; Tryk, D. A. *J. Photochem. Photobiol., A* **2000**, *1*, 1.
(12) Yamabi, S.; Imai, H. *Chem. Mater.* **2002**, *14*, 609.
(13) Gong, D.; Grimes, C. A.; Varghese, O. K.; Hu, W. C.; Singh, R. S.; Chen, Z.; Dickey, E. C. *J. Mat. Res.* **2001**, *16*, 3331.
(14) Ruan, C.; Paulose, M.; Varghese, O. K.; Mor, G. K.; Grimes, C. A. *J. Phys. Chem. B* **2005**, *109*, 15754.
(15) Allam, N. K.; Grimes, C. A. *J. Phys. Chem. C* **2007**, *111*, 13028.
(16) Allam, N. K.; Shankar, K.; Grimes, C. A. *Adv. Mater.* **2008**, *20*, 3942.
(17) Yoriya, S.; Paulose, M.; Varghese, O. K.; Mor, G. K.; Grimes, C. A. *J. Phys. Chem. C* **2007**, *111*, 13770.
(18) Prakasam, H. E.; Shankar, K.; Paulose, M.; Varghese, O. K.; Grimes, C. A. *J. Phys. Chem. C* **2007**, *111*, 7235.
(19) Allam, N. K.; Grimes, C. A. *Sol. Energy Mater. Sol. Cells* **2008**, *92*, 1468.
(20) Grimes, C. A. *J. Mat. Chem.* **2007**, *17*, 1451.
(21) Mor, G. K.; Varghese, O. K.; Paulose, M.; Shankar, K.; Grimes, C. A. *Sol. Energy Mater. Sol. Cells* **2006**, *90*, 2011.
(22) Varghese, O. K.; Gong, D. W.; Paulose, M.; Grimes, C. A.; Dickey, E. C. *J. Mat. Res.* **2003**, *18*, 156.
(23) Yang, Y.; Wang, X.; Li, L. *J. Am. Ceram. Soc.* **2008**, *91*, 632.
(24) Chen, C.-C.; Chen, J.-H.; Chao, C.-G.; SAY, W. C. *J. Mat. Sci.* **2005**, *25*, 4053.
(25) Akita, T.; Okumura, M.; Tanaka, K.; Ohkuma, K.; Kohyama, M.; Koyanagi, T.; Date, M.; Tsubota, S.; Haruta, M. *Surf. Interface Anal.* **2005**, *37*, 265.
(26) Mor, G. K.; Shankar, K.; Paulose, M.; Varghese, O. K.; Grimes, C. A. *Nano Lett.* **2005**, *5*, 191.
(27) Mor, G. K.; Prakasam, H. E.; Varghese, O. K.; Shankar, K.; Grimes, C. A. *Nano Lett.* **2007**, *7*, 2356.
(28) Grimes, C. A.; Varghese, O. K.; Ranjan, S. *Light, Water, Hydrogen: The Solar Production of Hydrogen by Water Photoelectrolysis*; Springer: Norwell, MA, 2007.
(29) Nishikiori, H.; Qian, W.; El-Sayed, M. A.; Tanaka, N.; Fujii, T. *J. Phys. Chem. C* **2007**, *111*, 9008.
(30) Kondo, J. N.; Domen, K. *Chem. Mater.* **2008**, *20*, 835.
(31) Paulose, M.; Shankar, K.; Yoriya, S.; Prakasam, H. E.; Varghese, O. K.; Mor, G. K.; Latempa, T. A.; Fitzgerald, A.; Grimes, C. A. *J. Phys. Chem. B* **2006**, *110*, 16179.
(32) Klug, H. P.; Alexander, L. E. *X-ray Diffraction Procedures for Polycrystalline and Amorphous Materials*; Wiley-Interscience: New York, 1974.
(33) Fujishima, A.; Zhang, X.; Tryk, D. A. *Surf. Sci. Rep.* **2008**, *63*, 515.
(34) Varghese, O. K.; Grimes, C. A. *Sol. Energy Mater. Sol. Cells* **2008**, *92*, 374.
(35) Allam, N. K.; Feng, X. J.; Grimes, C. A. *Chem. Mater.* **2008**, *20*, 6477.

JP902140D